

# Homeodomain transcription factor and tumor suppressor *Prep1* is required to maintain genomic stability

Giorgio Iotti<sup>1</sup>, Elena Longobardi<sup>1</sup>, Silvia Masella, Leila Dardaei, Francesca De Santis, Nicola Micali, and Francesco Blasi<sup>2</sup>

IFOM Istituto FIRC (Fondazione Italiana per la Ricerca sul Cancro) di Oncologia Molecolare, 20139 Milan, Italy

Edited\* by Ira Pastan, National Cancer Institute, National Institutes of Health, Bethesda, MD, and approved June 8, 2011 (received for review April 4, 2011)

***Prep1* is a homeodomain transcription factor that is essential in embryonic development and functions in the adult as a tumor suppressor. We show here that *Prep1* is involved in maintaining genomic stability and preventing neoplastic transformation. Hypomorphic homozygous *Prep1<sup>hi</sup>* fetal liver cells and mouse embryonic fibroblasts (MEFs) exhibit increased basal DNA damage and normal DNA damage response after  $\gamma$ -irradiation compared with WT. Cytogenetic analysis shows the presence of numerous chromosomal aberrations and aneuploidy in very early-passage *Prep1<sup>hi</sup>* MEFs. In human fibroblasts, acute *Prep1* down-regulation by siRNA induces DNA damage response, like in *Prep1<sup>hi</sup>* MEFs, together with an increase in heterochromatin-associated modifications: rapid increase of histone methylation and decreased transcription of satellite DNA. Ectopic expression of *Prep1* rescues DNA damage and heterochromatin methylation. Inhibition of Suv39 activity blocks the chromatin but not the DNA damage phenotype. Finally, *Prep1* deficiency facilitates cell immortalization, escape from oncogene-induced senescence, and H-Ras<sup>V12</sup>-dependent transformation. Importantly, the latter can be partially rescued by restoration of *Prep1* level. The results show that the tumor suppressor role of *Prep1* is associated with the maintenance of genomic stability.**

Transcription factor *Prep1* belongs to the 3aa-loop extension class of homeodomain proteins and is essential at multiple stages of embryonic development (1–4). *Prep1* is ubiquitously expressed both in developing and adult mice and can form tripartite DNA-binding complexes with members of the *Hox* and *Pbx* protein families (5–7). Furthermore, *Prep* and *Pbx* interact in the absence of DNA, and this interaction regulates the subcellular localization (8) and stability (9) of *Pbx* proteins.

In the zebrafish, down-regulation of *Prep1.1* is lethal to embryos (1); in the mouse, *Prep1*-null embryos die before gastrulation, because epiblast cells undergo *p53*-dependent apoptosis (4). Mouse embryos carrying a hypomorphic *Prep1<sup>hi</sup>* mutation (expressing 2% mRNA and 3–7% protein compared with WT) show general organ hypoplasia and in 75% of cases, die at about embryonic day E17.5 with major alterations in hematopoiesis, angiogenesis, and eye development (2, 10). Furthermore, *Prep1<sup>hi</sup>* mouse embryonic fibroblasts (MEFs) show increased basal and genotoxic stress-induced apoptosis (11). Remarkably, the homozygous *Prep1<sup>hi</sup>* hypomorphic mice that survive embryonic lethality are prone to develop tumors late in life, suggesting that *Prep1* may be a tumor suppressor in mice (12). Indeed, *Prep1* haploinsufficiency accelerates the development of the *EμMyc* lymphomas, and a survey of human cancers shows a dramatic reduction of *Prep1* expression in a large proportion (70%) of the patients (12).

Additionally, literature data are consistent with this conclusion. Human *PREP1* (mapping on chromosome 21 from 43.267712 to 43.326757 Mb) (13) is included in a region that undergoes loss of heterozygosity in 31% of informative breast cancers (14) and 50% of informative gastric cancers (15).

The presence of genetic instability is a hallmark of cancer, frequently manifested as aneuploidy (16–18). The late development of tumors in the *Prep1<sup>hi</sup>* hypomorphic mice surviving em-

brionic lethality (12), the *p53*-dependent apoptosis of the *Prep1*-null epiblast (4), and the apoptosis in the *Prep1<sup>hi</sup>* MEFs (11) suggest that genetic instability might be a basic cellular phenotype associated with *Prep1* down-regulation/absence.

We have, therefore, studied the role of *Prep1* in maintaining genetic stability and found that *Prep1*-deficient cells exhibit increased DNA damage with consequent alterations in chromatin methylation and satellites transcription, chromosomal aberrations, escape from H-Ras<sup>V12</sup>-induced senescence, and increased susceptibility to H-Ras<sup>V12</sup>-dependent neoplastic transformation.

## Results

***Prep1<sup>hi</sup>* Cells Accumulate DNA and Chromosomal Damage.** *Prep1<sup>hi</sup>* cells present evidence of basal activation of the DNA damage response (DDR) pathway. We measured (by immunofluorescence) Atm and H2AX phosphorylation foci (19–21) in second-passage MEFs derived from littermate WT and *Prep1<sup>hi</sup>* embryo pairs. Fig. 1, *Upper* shows representative immunofluorescence pictures with  $\gamma$ H2AX or phospho-Atm antibodies. The histograms in Fig. 1, *Lower* show that *Prep1<sup>hi</sup>* cultures display more DNA damage foci per cell than WT (Fig. 1, *Lower Left*) as well as a higher proportion of cells with more than two foci (Fig. 1, *Lower Right*).

The observation was not limited to fibroblasts, because *Prep1<sup>hi</sup>* fetal liver (FL) cells also present evidence of DNA damage in an alkaline Comet assay. Typical results for WT and *Prep1<sup>hi</sup>* FL cells are shown in Fig. S1. We observed a greater number of long comets (DNA strand breaks) in *Prep1<sup>hi</sup>* than in WT FL cells. Quantification of the results confirmed that *Prep1<sup>hi</sup>* cells have a higher basal level of DNA damage than WT FL cells, which is intermediate between untreated and  $\gamma$ -irradiated WT cells (positive control). Overall, this result also supports the above data and suggests that the activation of Atm (Fig. 1) was the consequence of genomic damage.

Fig. 2*A* shows the time course of  $\gamma$ H2AX foci formation after irradiation. Representative pictures (at 0 and 15 min after irradiation) are shown (Fig. 2*A*, *Upper*). The histogram (Fig. 2*A*, *Lower*) shows that the number of  $\gamma$ H2AX foci increased with time, peaked at 2 h, and then, decreased to almost basal level. From 0 to 6 h, the number of foci in *Prep1<sup>hi</sup>* MEFs was twofold larger than in WT littermate cells. The stronger response of *Prep1<sup>hi</sup>* MEFs to irradiation may be related to the higher basal

Author contributions: G.I., E.L., and F.B. designed research; G.I., E.L., S.M., L.D., and F.D.S. performed research; N.M. contributed new reagents/analytic tools; G.I., E.L., L.D., and F.B. analyzed data; and G.I. and F.B. wrote the paper.

The authors declare no conflict of interest.

\*This Direct Submission article had a prearranged editor.

Freely available online through the PNAS open access option.

<sup>1</sup>G.I. and E.L. contributed equally to this work.

<sup>2</sup>To whom correspondence should be addressed. E-mail: francesco.blasi@ifom-ieo-campus.it.

See Author Summary on page 11739.

This article contains supporting information online at [www.pnas.org/lookup/suppl/doi:10.1073/pnas.1105216108/-DCSupplemental](http://www.pnas.org/lookup/suppl/doi:10.1073/pnas.1105216108/-DCSupplemental).

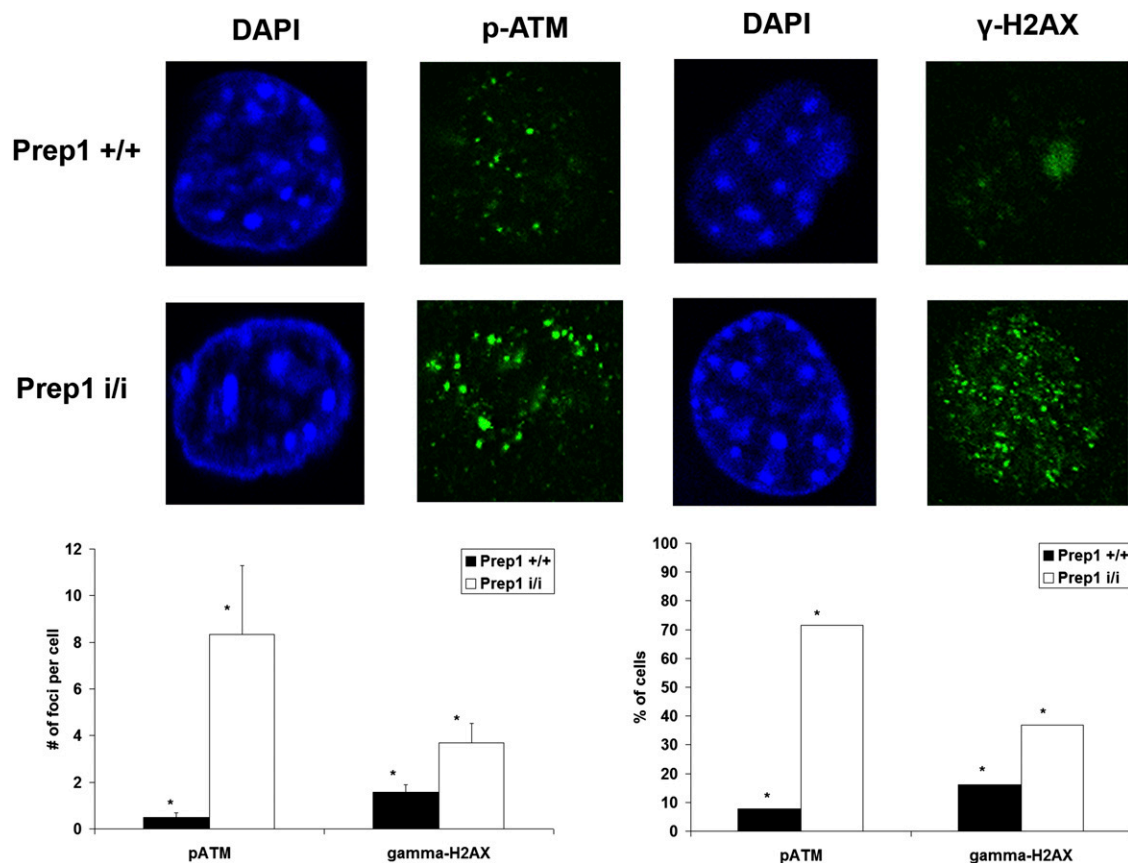


**Fig. 1.** Evidence of basal DNA damage in *Prep1<sup>ii</sup>* cells. Immunofluorescence analysis of WT and *Prep1<sup>ii</sup>* MEFs with DAPI,  $\gamma$ -H2AX, and phospho-Atm (Atm-S1981P) antibodies. (Upper) Representative examples. (Lower) The histograms show (Left) the averaged quantitation from two experiments comparing WT and *Prep1<sup>ii</sup>* cells (at least 50 cells per slide were analyzed;  $*P < 0.01$ ) and (Right) the proportion of analyzed cells of the indicated genotype that display more than two phospho-Atm or  $\gamma$ -H2AX foci ( $*P < 0.01$  for the comparison between WT and *Prep1<sup>ii</sup>* MEFs; Fisher exact test).

number of  $\gamma$ H2AX foci. These results suggest that *Prep1<sup>ii</sup>* MEFs have an efficient DNA repair machinery.

These results were confirmed by immunoblotting using anti- $\gamma$ H2AX and antiphospho-Atm antibodies (Fig. 2B). The phosphorylation of p53, one of the targets of Atm kinase (22, 23), was not reproducibly different in untreated WT vs. *Prep1<sup>ii</sup>* cells, but it peaked after irradiation, confirming a strong DNA damage-associated response in *Prep1*-deficient cells (Fig. S24). Furthermore, phosphorylation of Atm targets (immunofluorescence with antiphospho-S/T-Q antibody) (Fig. S2B) was also increased in *Prep1<sup>ii</sup>* cells.

Flow cytometric analysis showed that *Prep1<sup>ii</sup>* MEFs had a higher DNA content than WT cells. In third-passage MEFs, we observed that 11.4% (5.5% in WT) of the cell population had a DNA content greater than  $4n$  (Fig. S3).

Overall, these results suggest that low *Prep1* expression may be associated with chromosomal instability. Indeed, karyotyping of three independent passage-0 E14.5 MEF cultures showed aneuploidy and chromosome structural aberrations in 39% of the *Prep1<sup>ii</sup>* cells compared with less than 21% of WT (Fig. 3A). Anomalies included tetraploidy without centromere division, chromosome fusions, Robertsonian centromere fusions, and miniature chromosomes (examples in Fig. 3B). Moreover, measurement of the chromosome number of three passage-5 WT and *Prep1<sup>ii</sup>* littermate MEFs also showed (Fig. 3C) that *Prep1<sup>ii</sup>* cells had a reduced proportion of euploid karyotypes (41% vs. 62%) than WT. The aneuploidy of *Prep1<sup>ii</sup>* MEFs is consistent with genetic instability.

**DNA Damage and Chromatin Modifications Are Rapid Consequences of the Down-Regulation of *Prep1*.** To distinguish whether the observed DNA damage is an early or late indirect consequence of the absence of *Prep1*, we down-regulated *Prep1* in normal human BJ fibroblasts by transfecting specific siRNAs. Two different *Prep1* siRNA oligonucleotides (Table S1) efficiently down-regulated *Prep1* (Fig. S4). Luciferase siRNA was used as control.

Twenty-four hours after transfection (time 0), the number of immunofluorescent phospho-S/T-Q and  $\gamma$ -H2AX-positive foci was higher in *Prep1*-silenced cells than in the luciferase control (Fig. 4A). In addition, 2 h after  $\gamma$ -irradiation ( $t = 26$  h), the response was stronger in *Prep1*-silenced cells. Densitometric analysis of immunoblotting confirmed that the level of  $\gamma$ -H2AX was higher in *Prep1*-silenced cells and increased upon irradiation (Fig. 4B). These recapitulate the results observed in MEFs.

Overall, these data point to a structural DNA-protecting role of *Prep1*. Because chromatin structure has a crucial role in the processes involved in DNA damage detection and signal propagation (24), we investigated *Prep1* localization in the nucleus in relation to heterochromatin and the effects of *Prep1* down-regulation on histone modifications. Immunofluorescence analysis of *Prep1* in BJ cells shows that *Prep1* was excluded from regions strongly stained with DAPI (i.e., heterochromatin). In addition, nuclear *Prep1* and trimethylated H3K9 (H3K9Me3) staining were mutually exclusive (Fig. 5A). Transfection of *Prep1*-specific siRNAs in BJ cells and analysis of histone modifications by Western blotting (Fig. 5D) and immunofluorescence (Fig. 5B and C) showed that H3K9 and H4K20 trimethylation was much more abundant in cells lacking *Prep1* than in control cells.

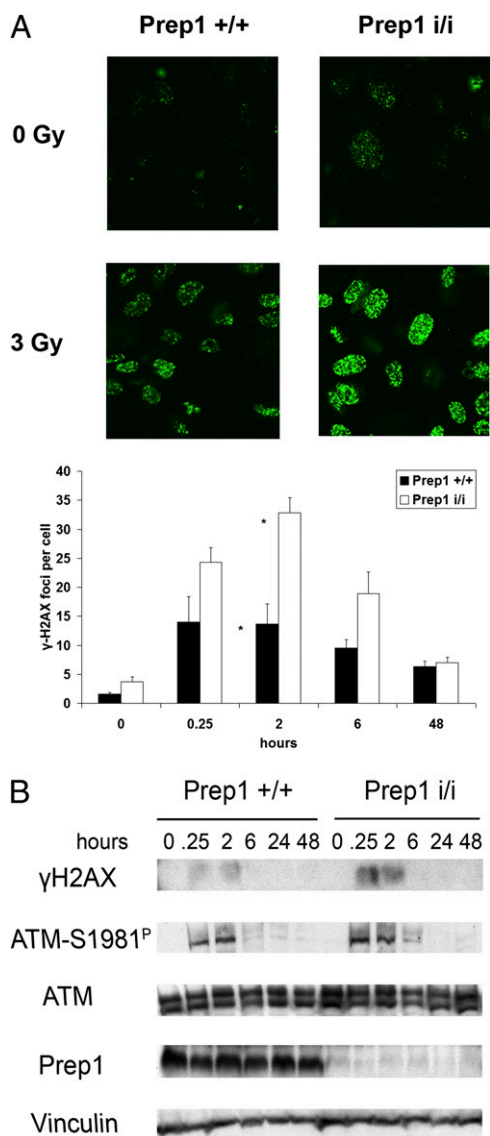


**Fig. 2.** *Prep1*<sup>+/+</sup> MEF response to radiation-induced DNA damage. (A) Time course by immunofluorescence of  $\gamma$ H2AX accumulation after  $\gamma$ -irradiation with 3Gy. At least 50 cells per slide were analyzed. \**P* < 0.01. (B) Immunoblotting analysis of extracts from WT and *Prep1*<sup>+/+</sup> MEFs at various times after 3Gy  $\gamma$ -irradiation, with specific anti- $\gamma$ H2AX, phospho-Atm, Atm, *Prep1*, and vinculin antibodies.

Ectopic expression of murine *Prep1* cDNA (not targetable by the human-specific *Prep1* siRNA1) completely rescued *Prep1*-dependent effects on both H3K9 methylation and DNA damage signaling (Fig. 5E).

Overall, therefore, down-regulation of *Prep1* rapidly induces DNA damage, activation of the DNA damage response, and chromatin modifications associated with heterochromatin.

***Prep1*-Deficient Cells Accumulate Trimethylated H3K9.** Epigenetics of chromatin is particularly important in maintaining its structure and genomic stability. Because repeated sequences represent a large fraction of the genome, their correct chromatin structure, replication, and expression are crucial in maintaining stability (25). To understand whether the chromatin modifications observed by immunoblotting in *Prep1* siRNA-transfected BJ cells are widespread or affect only specific regions of the genome, we performed ChIP experiments using anti-H3K9Me3 and anti-total H3 antibodies. Immunoprecipitated DNA was then analyzed by

real-time PCR with gene- or repeat-specific primers (26). *Prep1*<sup>+/+</sup> MEFs showed higher accumulation of H3K9 trimethylation in all analyzed elements, including tandem satellite repeats (major, 3.3-fold; minor, 2.2-fold), interspersed elements (SINE B1, threefold), and rDNA (2.9-fold) compared with WT (Table 1). The GAPDH promoter and the histone methyltransferase *Suv4-20h2* promoter also showed enrichment of H3K9me3 in *Prep1*<sup>+/+</sup> MEFs with respect to WT. Thus, *Prep1* deficiency results in a widespread increase of heterochromatin-associated repressive marks. This change might lead to compaction of chromatin, which was indicated by the higher enrichment by ChIP of total H3 in the analyzed genomic elements. These modifications were a direct early consequence of *Prep1* deficiency, because they could be recapitulated comparing ChIP experiments performed in control vs. *Prep1* siRNA-transfected human BJ cells (Table 2). Chromatin was obtained from control and *Prep1*-silenced (24 h) cells, immunoprecipitated with anti-H3K9Me3 and anti-total H3 antibodies, and purified DNA was amplified using primers specific for centromeric and pericentromeric satellite regions (27–29).

In mice, the pericentric compartment is composed of major satellite repeats, whereas minor satellites are localized in the centromere; both types of repeats are transcribed (30). The levels of RNA for major and minor satellites inversely correlate with the levels of *Suv39h*, which controls pericentric and centric H3K9 trimethylation (26). In humans, centromeric regions contain 171-bp AT (adenine-thymine)-rich  $\alpha$ -satellite motifs. The size and structure of pericentromeric regions varies between chromosomes, but in general, they are formed by GGAAT-rich satellite repeats of three types: I (0.5% of the genome), II (2% of the genome), and III (1.5% of the genome) (31).

Real-time RT-PCR of the major satellite transcript in MEFs showed a 60% reduction in *Prep1*<sup>+/+</sup> cells compared with WT (Table 3). Likewise, *Prep1*-dependent reduction of  $\alpha$ -satellite transcription (45% of control levels) was also observed in human BJ cells transfected with siRNAs (Table 3). However, the levels of *Suv39h.1* and *Suv39h.2* were not affected by *Prep1* (Fig. S5A).

The possibility that *Prep1* directly binds major satellite repeats was investigated by ChIP using anti-*Prep1* antibody in WT MEFs. Immunoprecipitated DNA was amplified with specific primers for major satellite and a region known to be bound by *Prep1* (*Suv4-20h2* promoter). As shown in Fig. S5B, unlike the positive control, no enrichment of the satellite repeat in *Prep1* antibody-immunoprecipitated chromatin was observed, excluding direct *Prep1* binding to pericentromeric satellites.

We conclude that the down-regulation of *Prep1* induces heterochromatin-like changes, with accumulation of H3K9 trimethylation and reduction of transcription of the satellite repeats.

**Chromatin Modifications Are a Consequence, Not the Cause, of the DNA Damage in *Prep1* Down-Regulated Cells.** We used the *Suv39* methyltransferase inhibitor chaetocin (SUVi) (32) to test whether the block of chromatin modifications would affect *Prep1* down-regulation-induced DNA changes. As shown in Fig. S6, chaetocin inhibited H3K9 trimethylation in *Prep1* down-regulated BJ cells. However, this treatment had no effect on the increase in  $\gamma$ -H2Ax induced by *Prep1* down-regulation. It seems, therefore, that the heterochromatin phenotype is a consequence rather than the cause of the DNA damage phenotype.

***Prep1*<sup>+/+</sup> MEFs Are More Susceptible to Oncogene-Induced Cell Transformation.** We analyzed the kinetics of immortalization of two WT and two *Prep1*<sup>+/+</sup> littermate MEF cultures using a 3T3 protocol. The population doubling level (PDL) (Fig. 6A) was identical in the two genotypes up to passage 9. From passages 9 to 34, WT MEFs grew with lower PDL than *Prep1*<sup>+/+</sup> MEFs. After passage 20, *Prep1*<sup>+/+</sup> MEFs markedly increased their proliferative capacity. Immunoblotting of whole extracts of WT and *Prep1*<sup>+/+</sup> MEFs at passages 5, 10, and 20 showed that, at early passages,

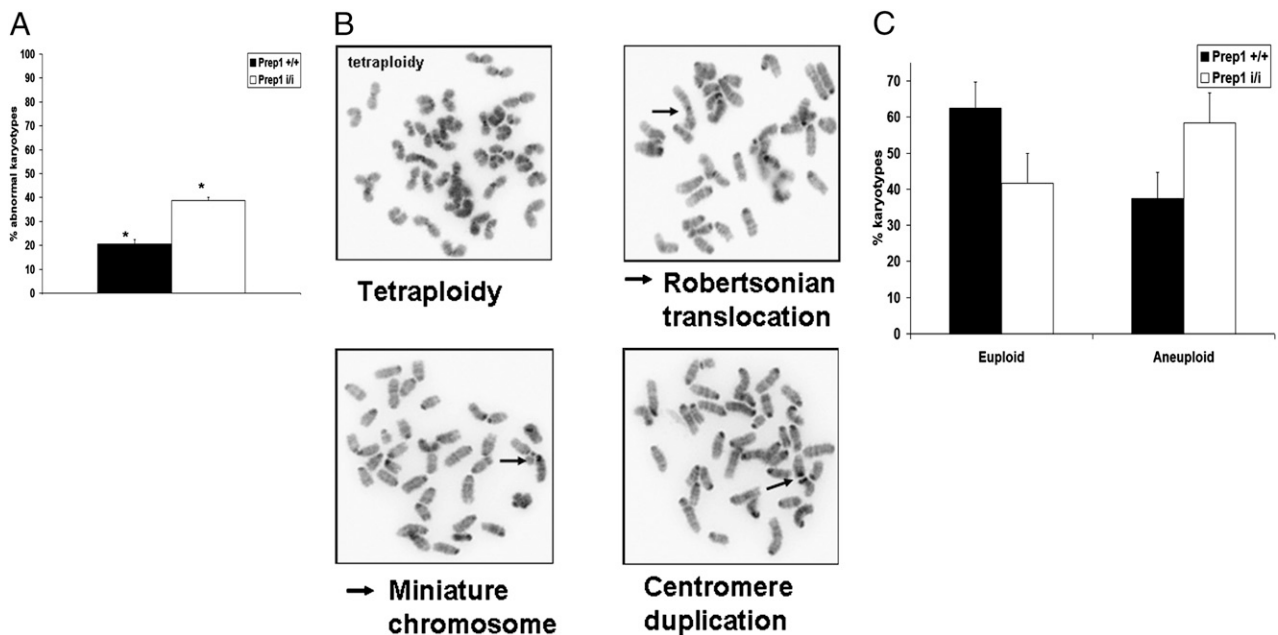


**Fig. 3.** *Prep1*<sup>ii</sup> MEFs accumulate more karyotypic abnormalities than WT. (A) Karyograms of three independent WT and three *Prep1*<sup>ii</sup> MEF lines were analyzed. The proportion of abnormal metaphases is significantly different between the genotypes. \**P* < 0.01. (B) The four pictures show different abnormalities in *Prep1*<sup>ii</sup> MEFs (indicated). (C) Karyotypes in passage-5 WT and *Prep1*<sup>ii</sup> MEFs (cell lines from three different littermate embryos of the two genotypes).

both *Prep1*<sup>ii</sup> MEF lines express high levels of p53, p16, and p19-ARF (*Ink4a* alternative reading frame coding for p19). However, these levels were strongly reduced at passage 20 (Fig. 6B).

The *trp53* and *Ink4a-Arf* loci are frequently altered during cultures of MEFs (33). PCR analysis of the *trp53* locus showed no anomalies in all analyzed MEF lines at passage 30 (Fig. 6C); consistently, we verified that the sequence of p53 mRNA was WT in these cells. However, in one of two *Prep1*<sup>ii</sup> MEF lines (*Prep1ii1*), PCR analysis of the *Ink4a-Arf* locus (1-kb region spanning exons 1 $\alpha$  and 1 $\beta$ ) at passage 30 did not provide any band, indicating a deletion of the gene (Fig. 6C). This finding agrees with the lack of expression of p16 and p19 (the ORFs encoded in the locus) by both RT-PCR (Fig. S7A) and immunoblotting (Fig. 7A). The loss of the *Ink4a-Arf* locus is additional evidence of the genomic instability of *Prep1*-deficient cells. Decreased expression of the growth regulators p53, p16, and p19

may explain the increased proliferative capacity of late-passage *Prep1*<sup>ii</sup> cells.

At passage 15, more *Prep1*<sup>ii</sup> MEFs incorporated BrdU than WT (47% vs. 31% of the cells) (Fig. S7B). Furthermore, *Prep1*<sup>ii</sup> MEFs had a higher cloning efficiency than WT (77  $\pm$  14 colonies vs. 43  $\pm$  14 colonies on plating of 5,000 cells) (Fig. S7C). Also, these data agree with the different kinetics of immortalization (Fig. 6A).

Transformation of primary rodent fibroblasts requires at least two oncogenes, whereas a single one is generally sufficient in immortalized cells (34, 35). Indeed, when either WT or *Prep1*<sup>ii</sup> passage-3 MEFs were infected with a retrovirus vector (pBabe Puro) encoding oncogenic *H-Ras*<sup>V12</sup>, we did not observe formation of either colonies in soft agar or tumors in mice (Fig. S7D). We, therefore, used immortalized MEFs to test whether *Prep1* could counteract *H-Ras*<sup>V12</sup>-dependent transformation. We transduced passage-30 MEFs with a retrovirus encoding oncogenic *H-Ras*<sup>V12</sup>

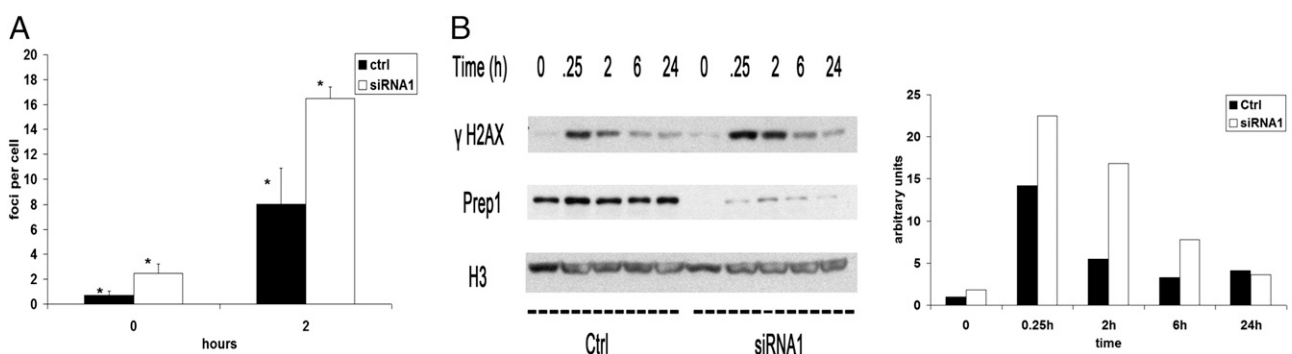


**Fig. 4.** The DNA damage response is activated immediately on *Prep1* down-regulation. (A) Quantitation of immunofluorescence analysis of DNA damage in BJ fibroblasts treated for 24 h with luciferase (Ctrl) or *Prep1*-specific siRNA oligonucleotide 1. At this time (time 0 in the figure), cells were  $\gamma$ -irradiated (3Gy). The histogram shows the number of colocalizing  $\gamma$ -H2AX and phospho-S/T-Q foci at time 0 and 2 h after  $\gamma$ -irradiation in control and down-regulated cells. At least 50 cells per slide were analyzed. \**P* < 0.05. (B Left) Immunoblotting of extracts of siRNA-transfected BJ cells at different times after  $\gamma$ -irradiation. (B Right) Densitometric analysis of phosphorylated H2AX (normalized to the levels of H3).

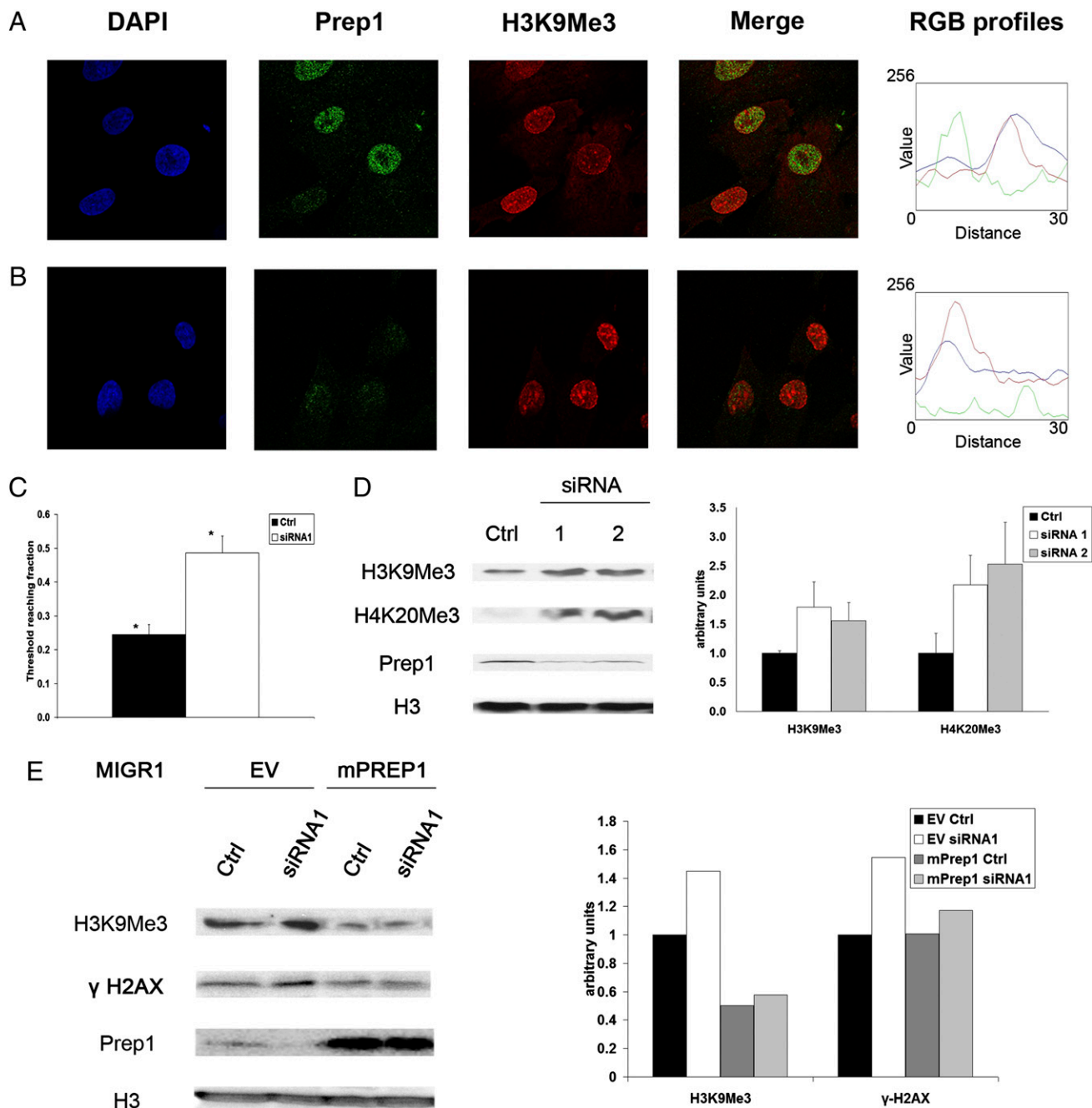


**Fig. 5.** Reduction of Prep1 is associated with increase in H3K9Me3 and H4K20Me3 levels. (A) Immunofluorescence analysis of BJ cells with DAPI, Prep1, and H3K9Me3 antibodies. In the RGB profile on the right, the blue line refers to DAPI, the green line refers to Prep1, and the red line refers to H3K9Me3 staining. (B) Immunofluorescent staining of BJ cells transfected with *Prep1* siRNA1. (C) The histogram shows the quantitation of the immunofluorescent staining. Differences between control and siRNA1 samples are evaluated comparing the fraction of the cell nuclei reaching a threshold H3K9Me3 staining. At least 40 cells per sample were analyzed. \* $P < 0.001$ . (D) Representative immunoblotting (Left) and densitometric analysis (Right) of lysates of BJ cells treated with control or *Prep1*-specific siRNAs. Specific anti-H3K9 Me3, H4K20 Me3, Prep1, and H3 antibodies were used. Densitometric analysis refers to three independent experiments (values are normalized to the levels of H3). (E) Immunoblotting (Left) and densitometric analysis (Right) of lysates of BJ cells transfected with MIGR1 EV or MIGR1 mPrep1 retroviruses and treated with control or Prep1 siRNA1. Specific anti-H3K9 Me3,  $\gamma$ -H2AX, Prep1, and H3 antibodies were used. For densitometric analysis, values are normalized to the levels of H3.

together with a MIGR1 (see *Materials and Methods*) vector carrying human PREP1 cDNA (or an empty vector as control). Infected cells were sorted by GFP positivity, and Ras and Prep1 expression levels were confirmed by immunoblotting (Fig. 7A).

Ras-expressing *Prep1<sup>ii</sup>* MEFs formed colonies in agar sevenfold more efficiently than WT (Fig. 7B) and when injected in immunodeficient mice, formed more aggressive tumors as mea-

sured by volume and survival kinetics (Fig. 7C and D). Remarkably, ectopic expression of *Prep1* significantly decreased the capacity of *Prep1<sup>ii</sup>* MEFs to form soft agar colonies in both lines (Fig. 7B) and decreased tumor growth of the *Prep1<sup>ii/2</sup>* line (Fig. 7C). The small difference in tumor volume in mice injected with WT Ras-transformed MEFs is not significant ( $P = 0.66$ ). Thus, on one hand, the genetic instability of *Prep1<sup>ii</sup>* MEFs favored

**Table 1. Altered chromatin modifications of repeated sequences in WT and *Prep1<sup>+/i</sup>* fibroblasts**

Element	H3K9me3		H3	
	WT	<i>Prep1<sup>i/i</sup></i>	WT	<i>Prep1<sup>i/i</sup></i>
Major satellite	0.117 ± 0.052	0.384 ± 0.075*	0.067 ± 0.033	0.142 ± 0.067
Minor satellite	0.154 ± 0.026	0.335 ± 0.027*	0.055 ± 0.014	0.098 ± 0.009
SINE B1	0.032 ± 0.006	0.096 ± 0.015*	0.065 ± 0.002	0.157 ± 0.015
rDNA	0.081 ± 0.005	0.232 ± 0.084	0.095 ± 0.005	0.152 ± 0.016
GAPDH	0.019 ± 0.006	0.049 ± 0.003*	0.042 ± 0.007	0.075 ± 0.010
Suv4-20	0.005 ± 0.002	0.017 ± 0.008	0.010 ± 0.002	0.017 ± 0.002

Immunoprecipitation of WT and *Prep1<sup>i/i</sup>* MEF chromatin with antibodies detecting H3K9me3 and total H3. Purified DNA from enriched chromatin fragments was amplified by real-time PCR with the repeat-specific primer sets. Relative enrichment referred to input amplification is shown. The results are representative of two independent experiments.

\* $P < 0.01$ .

*H-Ras<sup>V12</sup>*-mediated transformation, but on the other hand, restoration of *Prep1* level counteracted transformation.

***Prep1* Down-Regulation Counteracts Oncogene-Induced Senescence in Normal Human Fibroblasts.** To understand whether the reduction of *Prep1* had a biological role in human cells as well, we stably knocked down *Prep1* in BJ fibroblasts using two independent shRNAs. We did not observe changes in cell growth rate in *Prep1*-silenced cells for at least six population doublings (Fig. S8A). Cells were infected with a retrovirus vector (pBabe Hygro) encoding oncogenic *H-Ras<sup>V12</sup>* (Fig. 8A) and subjected to BrdU incorporation and colony-forming assays. Ras induces senescence in normal human fibroblasts (36) (Fig. S8B); consistently, Ras expression reduced the proportion of BrdU-incorporating cells in an 8-h pulse experiment. Remarkably, the effect was

**Table 2. Altered chromatin modifications of repeated sequences in *Prep1* siRNA-treated human fibroblasts**

Element	H3K9me3		H3	
	Control	siRNA1	Control	siRNA1
$\alpha$ -Sat	0.451 ± 0.006	0.721 ± 0.064*	0.130 ± 0.008	0.150 ± 0.005
SatII	0.493 ± 0.010	0.760 ± 0.025*	0.066 ± 0.006	0.101 ± 0.004
SatIII	0.811 ± 0.058	1.21 ± 0.073*	0.068 ± 0.010	0.106 ± 0.011

Control and *Prep1* siRNA1-transfected BJ cell chromatin was immunoprecipitated with antibodies detecting H3K9me3 and total H3. Purified DNA from enriched chromatin fragments was amplified by real-time PCR with the repeat-specific primer sets. Relative enrichment referred to input amplification is shown. The results are representative of two independent experiments.

\* $P < 0.01$ .

stronger in the control population (5.5-fold reduction) than in cells knocked down for *Prep1* (2.7-fold) (Fig. 8B), suggesting the presence of a fraction of cells bypassing the effect of the oncogene. Indeed, Ras-expressing *Prep1*-silenced cells were fourfold more clonogenic than controls (Fig. 8C), despite similar Ras expression and activity (measured by phospho-Erk1/2 levels) (Fig. 8A). The biological behavior of *Prep1*-silenced cells is consistent with reduced levels of p53 and ARF compared with controls, indicating that the oncogene-induced checkpoint in normal cells is defective on down-regulation of *Prep1*. This finding suggests that the reduction of *Prep1* interferes with the oncogene-induced senescence in human cells.

## Discussion

Genetic instability is a common feature in cancer and, in fact, mutations in genes involved in processes like DNA repair, chromosomal segregation, checkpoint control, and centrosome duplication are oncogenic (37, 38). Many tumor suppressor genes are specialized in controlling these processes. We now show that the tumor suppressor *Prep1* (12) prevents genetic instability.

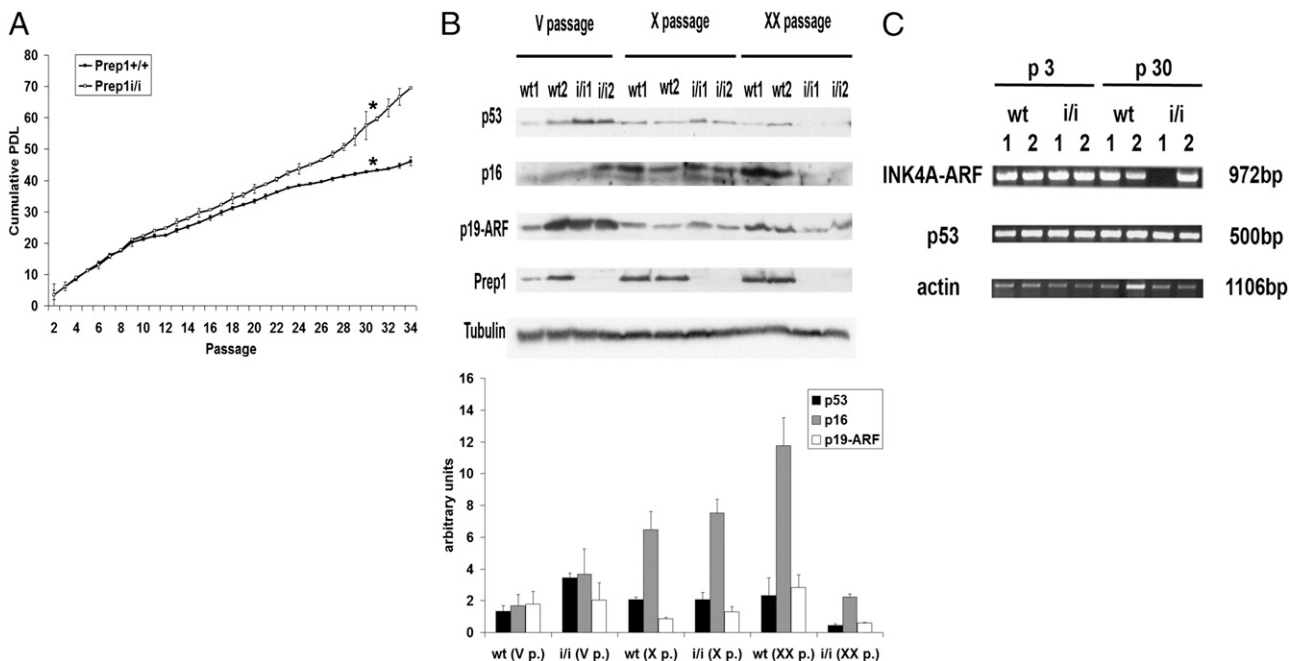


**Fig. 6.** Early immortalization and INK4A-ARF deletion in *Prep1<sup>+/i</sup>* MEFs. (A) Cell proliferation by a 3T3 protocol: averaged growth curves from two individually derived primary MEFs of each genotype (error bars indicate SEM; \* $P < 0.05$ ). (B) Immunoblotting (Upper) and densitometric analysis (Lower) of lysates of different passage MEFs for p53, p16, p19-ARF, and *Prep1* using tubulin as a protein loading control. (C) PCR analysis of genomic DNA of passage-3 and -30 (p3 and p30) WT or *Prep1<sup>+/i</sup>* MEFs. Intronic regions of *INK4A-ARF*, *p53*, and  $\beta$ -*ACTIN* loci were amplified (Table S1).

**Table 3. Decreased satellite transcription in *Prep1<sup>ii</sup>* and human *Prep1*-specific siRNA-treated fibroblasts**

Repeated sequence	N	Cells	Percent of control	P value
Major satellite	3	MEFs	37.7 ± 3.9	0.04
α-satellite	4	BJ	55.5 ± 5.8	0.02

Real-time RT-PCR analysis for satellite repeat-derived transcript levels in mouse *Prep1<sup>ii</sup>* vs. WT MEFs or in human BJ fibroblasts transfected with two different *Prep1*-specific siRNAs vs. control siRNA. The data are expressed as percent of WT or siRNA controls after normalization for the housekeeping gene expression. N indicates the number of experiments.

*Prep1* is essential at different stages of embryonic development and in the adult. The DNA-protecting role of *Prep1* may be essential already at the epiblast stage, when *Prep1* null embryos die (4). In agreement with this hypothesis, epiblast cell apoptosis requires p53 and is facilitated in the absence of *Atm* (4). In addition, *Prep1* exerts more multiple functions at later stages in development.

The genetic instability of *Prep1*-deficient cells is shown by increased DNA damage response foci, aneuploidy, chromosomal aberrations, and susceptibility to oncogene-mediated transformation. The DNA damage-dependent signaling pathway is strongly activated in *Prep1<sup>ii</sup>* cells, and the DNA repair seems to be efficient. Thus, the DNA damage phenotype can explain the p53-dependent apoptosis of the *Prep1* null epiblast and its exacerbation in the absence of *Atm* (4). Genetic instability is not the

consequence of prolonged propagation in culture of *Prep1<sup>ii</sup>* cells, because early-passage MEFs already exhibit evidence of chromosomal instability (Fig. 3A), and the DNA damage and DNA damage response are induced in human cells early after *Prep1* down-regulation (Fig. 4).

We hypothesize that *Prep1*-deficient cells undergo continuous cycles of double strand-break formation and repair, a condition that would lead to the genomic instability that is characteristic of many precancerous lesions (39, 40). The question, therefore, becomes whether *Prep1* deficiency directly increases DNA damage or causes replication stress (41, 42).

Many of the observed properties, such as aneuploidy, are similar to those observed in MEFs null for the p53 alleles (43, 44). Nevertheless, unlike p53<sup>-/-</sup> MEFs, which exhibit an increased rate of proliferation compared with control cells (43), early-passage *Prep1<sup>ii</sup>* MEFs proliferate at a similar rate as WT (Fig. 6A). The enhanced proliferative potential of *Prep1<sup>ii</sup>* MEFs seems concomitant to reduced expression of p53, p16, and p19 and occurs at later passages (Fig. 6A and B). Thus, the reduction of *Prep1* renders cells genetically unstable, favoring loss of checkpoint genes like *Ink4a-Arf* and the subsequent transformed phenotype. However, this is an indirect effect of *Prep1*, because no regulation of either p16 or p19 is observed in early-passage MEFs (Fig. 6B).

Why does *Prep1* deficiency result in genetic instability? The effect of *Prep1* down-regulation on chromatin methylation and expression of the satellite DNA might suggest a possible mechanism. In *Drosophila*, the deletion of the single ortholog of both

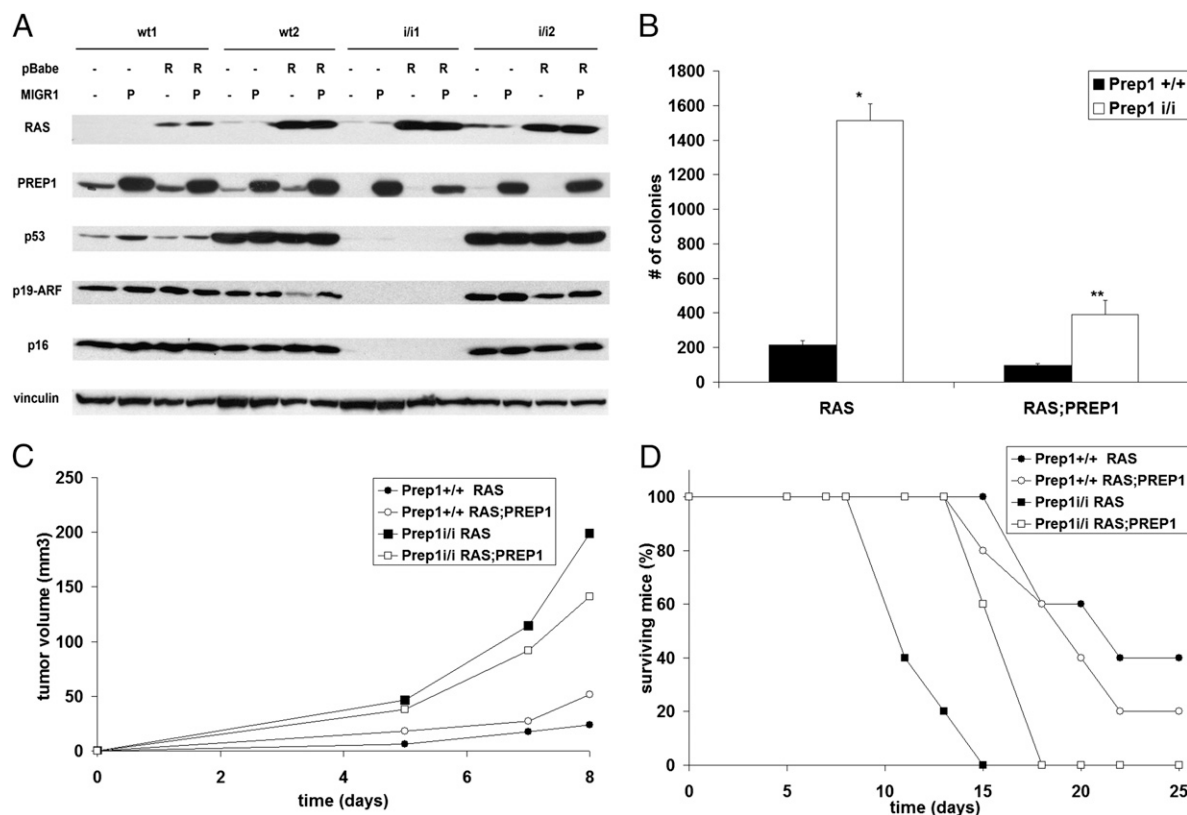


**Fig. 7. Increased transformation susceptibility of *Prep1<sup>ii</sup>* MEFs. (A)** Expression levels of Ras, *Prep1*, p53, p16, and p19-ARF (Western blotting) of passage-30 MEFs infected with the indicated retroviruses (–, empty vector; R, Ras; P, *Prep1*). Vinculin was used as a protein loading control. (B) Anchorage-independent soft agar growth assay of retrotransduced MEFs. The number of colonies formed by 10<sup>5</sup> WT or *Prep1<sup>ii</sup>* MEFs per plate, infected with the indicated retroviruses, is shown (n = 5; \*P < 0.001 compared with WT MEFs; \*\*P < 0.001 compared with RAS-infected MEFs). (C and D) In vivo tumor growth rates (C) and survival kinetics (D) of immunocompromised mice injected s.c. with WT and *Prep1<sup>ii</sup>* MEFs (8 × 10<sup>5</sup> cells per animal) transduced with the indicated retroviruses. EV, empty vector. Lines represent the average of five animals per group. Differences between *Prep1* WT and *Prep1<sup>ii</sup>* (P < 0.01) and between *Prep1<sup>ii</sup>* RAS-EV and *Prep1<sup>ii</sup>* RAS-PREP1 (P < 0.05) groups are statistically significant.

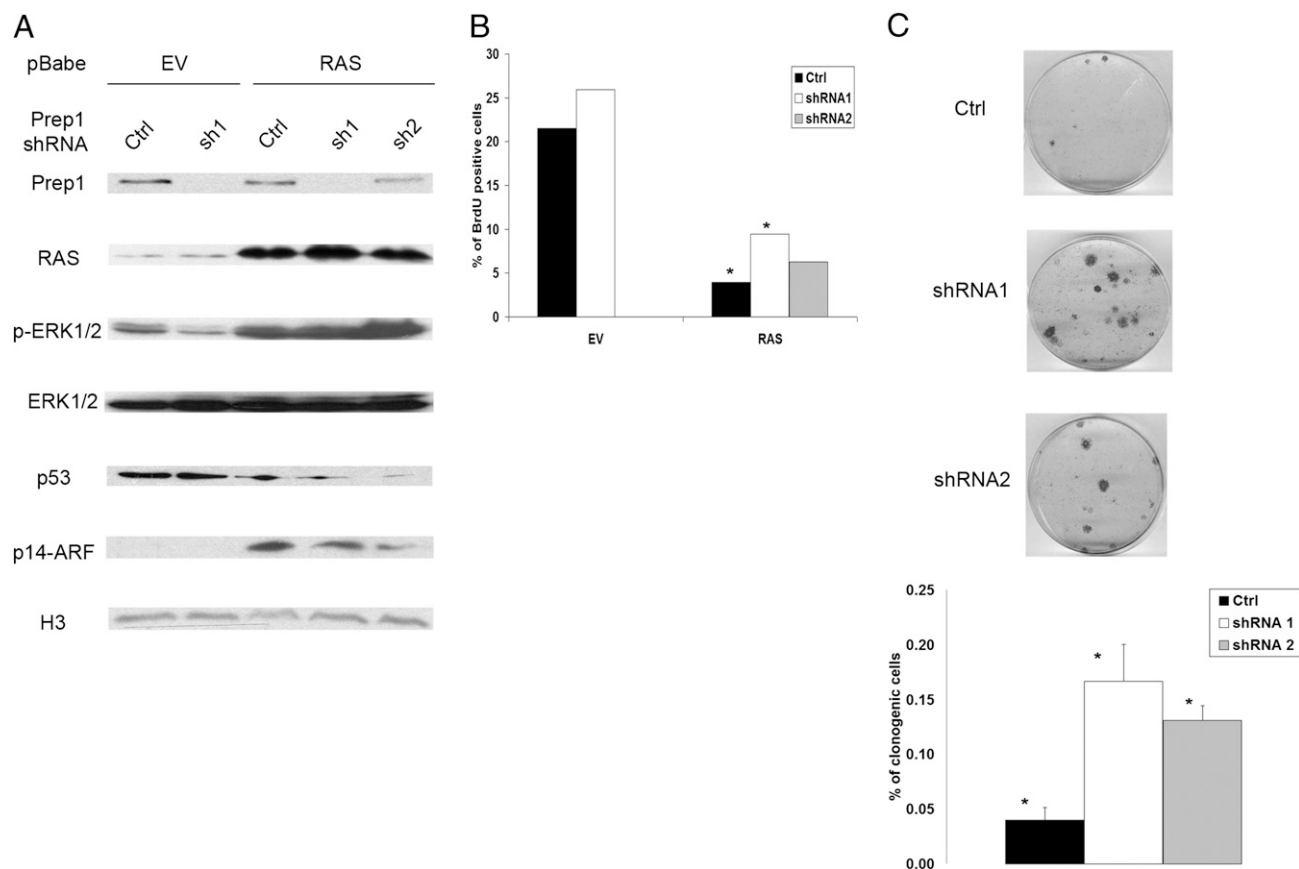


**Fig. 8.** Down-regulation of *Prep1* prevents oncogene-induced senescence. (A) The immunoblot shows the expression levels of *Prep1*, *Ras*, phospho-Erk1/2, Erk1/2, p53, and p14-ARF in BJ cells infected with the indicated retroviruses. Histone H3 is shown as a protein-loading control. (B) BrdU incorporation assay of *Ras*-expressing BJ cells. Data represent the proportion of BrdU-incorporating cells infected with the indicated retroviruses. At least 150 cells were analyzed for each sample. The experiment was repeated two times with similar results ( $*P < 0.05$ ; Fisher exact test). (C) Colony assay of *Ras*-expressing BJ cells. Upper shows representative examples of plates on seeding  $5 \times 10^3$  cells. The histogram in Lower shows the percent of clonogenic cells obtained in two independent experiments performed seeding three cell doses ( $2 \times 10^3$ ,  $5 \times 10^3$ , and  $10^4$ ) in triplicate for each experiment ( $*P < 0.01$ ).

*Prep* and *Meis*, *Hth*, is accompanied by chromosomal instability and loss of transcription of pericentric satellite repeats (45). However, the effects of *Prep1* and *Hth* are different; whereas *Hth* physically interacts with RNA PolII in the satellite regions, *Prep1* does not bind to pericentric major satellites (Fig. S5B). It is interesting to notice that, in mammals, although *Prep1* is a tumor suppressor (12), the other *Hth* ortholog *Meis1* is, in fact, an oncogene, at least in hematopoietic malignancies (46, 47).

It has been recently shown that many human cancers display overexpression of satellite transcripts, which may reflect global alterations in heterochromatin silencing (48). This finding is the opposite of our observations (Fig. 5 and Tables 1–3). However, *Prep1* down-regulated cells are not yet transformed, and in any case, their chromatin modifications seem a consequence, not a cause, of the DNA damage (Fig. S6). Based on our observations, we hypothesize that the increase in heterochromatin markers observed in *Prep1* knock-down cells can actually be the consequence of an oncogene-like replication stress (49).

Because genomic instability highly increases the chance of accumulating genetic mutations, leading to cancer development (50), the present work provides a cellular basis for the identified tumor-suppressor activity of *Prep1* (12). Indeed, we present evidence that the reduction of *Prep1* compromises checkpoint mechanisms involved in limiting oncogene-induced transformation (Fig. 7) and establishing oncogene-induced senescence in human cells (Fig. 8). It is noteworthy that, despite the occurrence of irreversible genetic events (like the deletion of the *Ink4a-ARF*

locus) in *Prep1<sup>ii</sup>* MEFs, the cells still require reduction of *Prep1* to manifest the full transformation potential. Ectopic *Prep1* expression reverts some of the transformed properties of these cells (colony formation efficiency in agar) (Fig. 7), suggesting that *Prep1* restoration might have therapeutic effects in the fraction of human tumors (12) expressing very low levels of *Prep1*.

Alterations in pathways involved in maintenance of genomic integrity might also explain other phenotypes associated with *Prep1* deficiency. The activation of the DNA damage response correlates with age-associated functional impairment of hematopoietic stem cells (51, 52), and indeed, we find profound defects in the repopulation capacity of *Prep1*-deficient long-term repopulating hematopoietic stem cells (10). Furthermore, the accumulation of DNA damage and genetic instability is consistent with the early postimplantation developmental arrest of the homozygous null *Prep1* mutant (4, 53, 54). In the *Prep1* model, we observe that loss of *Atm* induces a phenotype as well in the otherwise normal heterozygous *Prep1<sup>+/-</sup>* embryos and worsens that of the homozygous *Prep1<sup>-/-</sup>* embryos (4). The stronger *Atm* activation in *Prep1<sup>ii</sup>* MEFs and the requirement of *Atm* to prevent a phenotype in the *Prep1<sup>+/-</sup>* epiblast (4) are consistent with the increased histone H3K9 and H4K20 methylation of *Prep1*-deficient cells (Fig. 5 C and D). Indeed, H3K9 and H4K20 trimethylation is a hallmark of heterochromatin, and *Atm* signaling is required to repair double-strand breaks associated with heterochromatin (55).

Based on the evidence acquired, it becomes central to identify the mechanisms linking *Prep1* to the stability of the genome to

explain the increased predisposition of *Prep1*-defective cells to transformation.

## Materials and Methods

*Prep1<sup>fl/fl</sup>* mice and embryos have been described (2). E14.5 WT and *Prep1<sup>fl/fl</sup>* MEFs were cultured under low oxygen tension. Unless otherwise specified, experiments were performed on MEFs at passage 2. BJ normal human fibroblasts (ATCC) were used at 30–35 population doublings. For serial 3T3 cultivation, cells were maintained on a defined 3-d schedule (3T3) by plating  $3 \times 10^5$  cells in 60-mm plate dishes. MIGR1 hPREP1 and MIGR1 mPREP1 were obtained by cloning human or mouse FLAG-tagged *Prep1* cDNA into the XhoI restriction site of the MIGR1 (MSCV-IRES-GFP) retroviral vector. COMET assay was performed as indicated in the manufacturer's protocol (Trevigen). Chromosome spreads were stained with DAPI (Sigma), and chromosome number and morphology were assessed with a 100 $\times$  objective Leica microscope with FishView software. For ChIP assays, cross-linked chromatin was immunoprecipitated with anti-H3K9Me3, mouse anti-H3, rabbit anti-Prep1, and anti-GFP (mock

control) antibodies. MEFs were infected with pBabe Puro empty vector (EV) or pBabe Puro H-Ras<sup>V12</sup> and with MIGR1 EV or MIGR1-PREP1 retroviruses. For soft agar assays, cells were seeded ( $10^5$  per plate in triplicate) in 35-mm soft agar dishes. For tumorigenicity assays,  $8 \times 10^5$  cells were injected s.c. into the flanks of athymic nude mice. The list of the oligonucleotides and of the antibodies employed in this paper is presented in [Tables S1 and S2](#).

Detailed information is included in [SI Materials and Methods](#).

**ACKNOWLEDGMENTS.** We are grateful to M. Foiani, F. D'Adda di Fagnagna, and S. Casola for stimulating scientific discussion. The help of the Fondazione Istituto FIRC (Fondazione Italiana per la Ricerca sul Cancro) di Oncologia Molecolare services (imaging and mouse husbandry) has been essential; we are grateful to A. Gobbi, M. Faretta, and D. Parazzoli for their help. The help of Omar Malazzi in karyotyping has been invaluable. G.I. was a recipient of an Italian Association for Cancer Research fellowship. This work was supported by grants from the Italian Association for Cancer Research, the Italian Ministry of Health, the Cariplo Foundation, and the FP7 program of European Union (Prepobedia) (all to F.B.).

- Deflorian G, et al. (2004) Prep1.1 has essential genetic functions in hindbrain development and cranial neural crest cell differentiation. *Development* 131:613–627.
- Ferretti E, et al. (2006) Hypomorphic mutation of the TALE gene Prep1 (pKnox1) causes a major reduction of Pbx and Meis proteins and a pleiotropic embryonic phenotype. *Mol Cell Biol* 26:5650–5662.
- Penkov D, et al. (2005) Involvement of Prep1 in the alphabeta T-cell receptor T-lymphocytic potential of hematopoietic precursors. *Mol Cell Biol* 25:10768–10781.
- Fernandez-Diaz LC, et al. (2010) The absence of Prep1 causes p53-dependent apoptosis of mouse pluripotent epiblast cells. *Development* 137:3393–3403.
- Ferretti E, Schulz H, Talarico D, Blasi F, Berthelsen J (1999) The PBX-regulating protein PREP1 is present in different PBX-complexed forms in mouse. *Mech Dev* 83:53–64.
- Ferretti E, et al. (2000) A complex site including both Pbx-Hox and Prep-Meis-responsive elements and binding a retinoic acid-inducible ternary Hoxb1-Pbx-Prep1 complex is required for HOXB2 rhombomere 4 expression. *Development*, 127, 155–166, 2000. *Development* 127:155–166.
- Jacobs Y, Schnabel CA, Cleary ML (1999) Trimeric association of Hox and TALE homeodomain proteins mediates Hox2 hindbrain enhancer activity. *Mol Cell Biol* 19:5134–5142.
- Berthelsen J, Kilstrup-Nielsen C, Blasi F, Mavilio F, Zappavigna V (1999) The subcellular localization of PBX1 and EXD proteins depends on nuclear import and export signals and is modulated by association with PREP1 and HTH. *Genes Dev* 13:946–953.
- Longobardi E, Blasi F (2003) Overexpression of PREP-1 in F9 teratocarcinoma cells leads to a functionally relevant increase of PBX-2 by preventing its degradation. *J Biol Chem* 278:39235–39241.
- Di Rosa P, et al. (2007) The homeodomain transcription factor Prep1 (pKnox1) is required for hematopoietic stem and progenitor cell activity. *Dev Biol* 311:324–334.
- Micali N, Ferrai C, Fernandez-Diaz LC, Blasi F, Crippa MP (2009) Prep1 directly regulates the intrinsic apoptotic pathway by controlling Bcl-XL levels. *Mol Cell Biol* 29:1143–1151.
- Longobardi E, et al. (2010) Prep1 (pKnox1)-deficiency leads to spontaneous tumor development in mice and accelerates EmMyc lymphomagenesis: A tumor suppressor role for Prep1. *Mol Oncol* 4:226–234.
- Berthelsen J, et al. (1998) PKNOX-1, a gene encoding Prep1, a new regulator of pbx activity, maps on human chromosome 21q22.3 and murine chromosome 17b/c. *Genomics* 47:323–324.
- Ohgaki K, et al. (1998) Mapping of a new target region of allelic loss to a 6-cM interval at 21q21 in primary breast cancers. *Genes Chromosomes Cancer* 23:244–247.
- Park WS, et al. (2000) Mapping of a new target region of allelic loss at 21q22 in primary gastric cancers. *Cancer Lett* 159:15–21.
- Rajagopalan H, Lengauer C (2004) Aneuploidy and cancer. *Nature* 432:338–341.
- Ganem NJ, Storchova Z, Pellman D (2007) Tetraploidy, aneuploidy and cancer. *Curr Opin Genet Dev* 17:157–162.
- Weaver BA, Cleveland DW (2007) Aneuploidy: Instigator and inhibitor of tumorigenesis. *Cancer Res* 67:10103–10105.
- Abraham RT (2001) Cell cycle checkpoint signaling through the ATM and ATR kinases. *Genes Dev* 15:2177–2196.
- Bassing CH, Alt FW (2004) H2AX may function as an anchor to hold broken chromosomal DNA ends in close proximity. *Cell Cycle* 3:149–153.
- Tanaka T, et al. (2007) Cytometry of ATM activation and histone H2AX phosphorylation to estimate extent of DNA damage induced by exogenous agents. *Cytometry A* 71:648–661.
- Banin S, et al. (1998) Enhanced phosphorylation of p53 by ATM in response to DNA damage. *Science* 281:1674–1677.
- Canman CE, et al. (1998) Activation of the ATM kinase by ionizing radiation and phosphorylation of p53. *Science* 281:1677–1679.
- van Attikum H, Gasser SM (2009) Crosstalk between histone modifications during the DNA damage response. *Trends Cell Biol* 19:207–217.
- Peng JC, Karpen GH (2008) Epigenetic regulation of heterochromatic DNA stability. *Curr Opin Genet Dev* 18:204–211.
- Martens JH, et al. (2005) The profile of repeat-associated histone lysine methylation states in the mouse epigenome. *EMBO J* 24:800–812.
- Guccione E, et al. (2007) Methylation of histone H3R2 by PRMT6 and H3K4 by an MLL complex are mutually exclusive. *Nature* 449:933–937.
- Gopalakrishnan S, Sullivan BA, Trazzi S, Della Valle G, Robertson KD (2009) DNMT3B interacts with constitutive centromere protein CENP-C to modulate DNA methylation and the histone code at centromeric regions. *Hum Mol Genet* 18:3178–3193.
- Valgardsdottir R, et al. (2008) Transcription of Satellite III non-coding RNAs is a general stress response in human cells. *Nucleic Acids Res* 36:423–434.
- Lehnertz B, et al. (2003) Suv39H-mediated histone H3 lysine 9 methylation directs DNA methylation to major satellite repeats at pericentric heterochromatin. *Curr Biol* 13:1192–1200.
- Eymery A, Callanan M, Vourc'h C (2009) The secret message of heterochromatin: New insights into the mechanisms and function of centromeric and pericentric repeat sequence transcription. *Int J Dev Biol* 53:259–268.
- Greiner D, Bonaldi T, Eskeland R, Roemer E, Imhof A (2005) Identification of a specific inhibitor of the histone methyltransferase SU(VAR)3-9. *Nat Chem Biol* 1:143–145.
- Kamijo T, et al. (1997) Tumor suppression at the mouse INK4a locus mediated by the alternative reading frame product p19<sup>ARF</sup>. *Cell* 91:649–659.
- Land H, Parada LF, Weinberg RA (1983) Tumorigenic conversion of primary embryo fibroblasts requires at least two cooperating oncogenes. *Nature* 304:596–602.
- Newbold RF, Overell RW (1983) Fibroblast immortality is a prerequisite for transformation by EJ c-Ha-ras oncogene. *Nature* 304:648–651.
- Serrano M, Lin AW, McCurrach ME, Beach D, Lowe SW (1997) Oncogenic ras provokes premature cell senescence associated with accumulation of p53 and p16INK4a. *Cell* 88:593–602.
- Lengauer C, Kinzler KW, Vogelstein B (1998) Genetic instabilities in human cancers. *Nature* 396:643–649.
- Negrini S, Gorgoulis VG, Halazonetis TD (2010) Genomic instability—an evolving hallmark of cancer. *Nat Rev Mol Cell Biol* 11:220–228.
- Bartkova J, et al. (2005) DNA damage response as a candidate anti-cancer barrier in early human tumorigenesis. *Nature* 434:864–870.
- Gorgoulis VG, et al. (2005) Activation of the DNA damage checkpoint and genomic instability in human precancerous lesions. *Nature* 434:907–913.
- Bartkova J, et al. (2006) Oncogene-induced senescence is part of the tumorigenesis barrier imposed by DNA damage checkpoints. *Nature* 444:633–637.
- Di Micco R, et al. (2006) Oncogene-induced senescence is a DNA damage response triggered by DNA hyper-replication. *Nature* 444:638–642.
- Harvey M, et al. (1993) In vitro growth characteristics of embryo fibroblasts isolated from p53-deficient mice. *Oncogene* 8:2457–2467.
- Fukasawa K, Wiener F, Vande Woude GF, Mai S (1997) Genomic instability and apoptosis are frequent in p53 deficient young mice. *Oncogene* 15:1295–1302.
- Salvany L, Aldaz S, Corsetti E, Azpiazu N (2009) A new role for hth in the early preblastodermic divisions in drosophila. *Cell Cycle* 8:2748–2755.
- Moskow JJ, Bullrich F, Huebner K, Daar IO, Buchberg AM (1995) *Meis1*, a *PBX1*-related homeobox gene involved in myeloid leukemia in BXH-2 mice. *Mol Cell Biol* 15:5434–5443.
- Lawrence HJ, et al. (1999) Frequent co-expression of the HOXA9 and MEIS1 homeobox genes in human myeloid leukemias. *Leukemia* 13:1993–1999.
- Ting DT, et al. (2011) Aberrant overexpression of satellite repeats in pancreatic and other epithelial cancers. *Science* 331:593–596.
- Di Micco R, et al. (2011) Interplay between oncogene-induced DNA damage response and heterochromatin in senescence and cancer. *Nat Cell Biol* 13:292–302.
- Halazonetis TD, Gorgoulis VG, Bartek J (2008) An oncogene-induced DNA damage model for cancer development. *Science* 319:1352–1355.
- Nijnik A, et al. (2007) DNA repair is limiting for haematopoietic stem cells during ageing. *Nature* 447:686–690.
- Rossi DJ, et al. (2007) Deficiencies in DNA damage repair limit the function of haematopoietic stem cells with age. *Nature* 447:725–729.
- Shen SX, et al. (1998) A targeted disruption of the murine Brca1 gene causes gamma-irradiation hypersensitivity and genetic instability. *Oncogene* 17:3115–3124.
- Brown EJ, Baltimore D (2000) ATR disruption leads to chromosomal fragmentation and early embryonic lethality. *Genes Dev* 14:397–402.
- Goodarzi AA, et al. (2008) ATM signaling facilitates repair of DNA double-strand breaks associated with heterochromatin. *Mol Cell* 31:167–177.